Guanine-Specific Chemical Reaction Reveals ssDNA Interactions on Carbon Nanotube Surfaces

Yu Zheng,[†,§] Ali A. Alizadehmojarad,[†] Sergei M. Bachilo,[†] and R. Bruce Weisman*[,†,‡]

[†] Department of Chemistry and the Smalley-Curl Institute, Rice University, Houston, TX 77005 United States

[‡] Department of Materials Science and NanoEngineering, Rice University, Houston, TX 77005 United States

ABSTRACT: Understanding the conformations of physisorbed single-stranded DNA (ssDNA) oligos on single-wall carbon nanotube (SWCNT) surfaces is important for advancing basic nanoscience and for developing applications in biomedicine and quantum information processing. Here we report evidence that the ssDNA strands are partly desorbed from the nanotube surface under common conditions. SWCNT suspensions were prepared in eight ssDNA oligos, each containing 1 guanine and 30 thymine bases but differing in the position of the guanine within the strand. Singlet oxygen exposure then covalently functionalized the guanine to the SWCNT surface, red-shifting the nanotube fluorescence by an amount reflecting the guanine spatial density at the surface. Spectral shifts were greatest for central guanine positions and smallest for end positions. In conjunction with steered molecular dynamics simulations, the results suggest that steric interference between neighboring ssDNA strands on an individual nanotube causes significant dislocation or desorption of the strand ends while central regions remain better wrapped around the nanotube. This effect decreases with decreasing concentrations of free ssDNA.

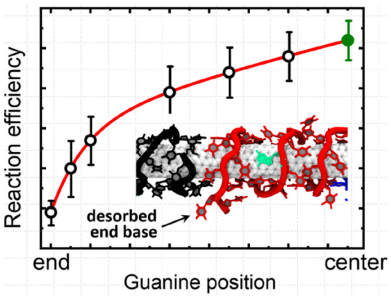

KEYWORDS: guanine-functionalized SWCNT, steered molecular dynamics, exciton trap, quantum defect, covalent functionalization

Single-wall carbon nanotubes (SWCNTs) are the most widely studied family of artificial one-dimensional nanomaterials. Their unique electronic and optical properties have commanded the interest of applied as well as basic researchers. Although all SWCNTs are nanoscale tubes composed of covalently linked carbon atoms, they assume a variety of discrete structures. Each such species is labeled by a pair of integers, (*n*,*m*), and has long-range internal order with a well-defined diameter, roll-up (chiral) angle, and characteristic physical and chemical properties.[1] Many SWCNT studies and applications require the nanotubes to be disaggregated and stably suspended in water with the aid of physisorbed surfactant or polymer coatings. Single-stranded DNA (ssDNA) has emerged as one of the most important nanotube coatings.[2] Selective interactions that depend on both the nucleobase sequence of the coating and the structure of the nanotube have allowed mixed nanotube samples to be (*n*,*m*)-sorted using ion exchange chromatography or aqueous two-phase extraction.[3–5] Such structural sorting is a key step for enabling many advanced SWCNT studies and applications. It has also been shown that ssDNA coatings can modulate nanotube optical properties in response to the presence of specific analytes, an effect that forms the basis for a promising class of bioanalytical sensors.[6–12] In addition, SWCNT-ssDNA hybrids have been used in the biotemplated nanofabrication of high performance field-effect transistors.[13,14] It is therefore clearly of interest to understand the factors controlling the structures of ssDNA coatings on SWCNTs.

Our current contribution toward this goal exploits the recent discovery that guanine nucleobases in ssDNA coatings selectively react in the presence of $^1O_2$ to form covalent bonds to the nanotube sidewall.[15] Unlike other covalent SWCNT reactions, this functionalization results in a high density of shallow exciton trap sites, whose collective depth and spatial pattern can be controlled through the choice of base sequence in the ssDNA oligo. As a result, the characteristic

SWCNT near-IR fluorescence becomes tunably red-shifted by amounts directly related to the guanine fraction in the ssDNA coating. In addition, guanine-functionalized SWCNTs (GF-SWCNTs) have been found to show single-photon emission as well as quantum coupling between distinct defect states within individual nanotubes, suggesting potential applications in quantum information processing.[16] Here we report results from a spectroscopic study of GF-SWCNTs combined with molecular dynamics simulations that give new insights into the structure of the ssDNA/SWCNT noncovalent precursors. Our results suggest that the ends of ssDNA strands in such systems are more likely to desorb from the SWCNT surface than central strand regions.

Our experiments used GF-SWCNTs prepared by the method reported earlier, in which singlet oxygen was generated by optical excitation of the sensitizer rose bengal.[15] The resulting functionalization reaction leads to SWCNT fluorescence spectral shifts that are nearly proportional to the fraction of guanine nucleotides in the ssDNA oligo coating (see Figure S3). It is thought that each guanine functionalization site causes a local perturbation to the nanotube π-electron system, forming a shallow trap for the mobile excitons. Because the spacing between nearby sites is smaller than the exciton size, they act collectively as deeper traps. This results in larger emission shifts that reflect the spatial density of functionalized guanine bases in the nanotube's ssDNA coating. The GF-SWCNTs differ qualitatively from SWCNTs covalently modified by sparse doping with oxygen atoms or functionalization with aryl groups, which introduce deeper, isolated exciton traps that give strongly red-shifted emission in parallel with normal E_{11} fluorescence from pristine regions.[17–23] By contrast, GF-SWCNTs show a single shifted emission feature that shifts smoothly from the E_{11} wavelength proportionally to the guanine density.[15] In the current study we compare those shifts for SWCNTs coated with different ssDNA isomers containing a single guanine plus

30 thymine bases. The primary finding is that spectral shifts depend systematically on the position of the guanine within the ssDNA strand.

Figure 1 shows the spectral changes caused by guanine functionalization in samples of SWCNTs dispersed by $T_{15}GT_{15}$ ssDNA oligos, which contain only one reactive nucleobase flanked by unreactive T_{15} tails that protect adjacent nanotube regions from functionalization. After treatment, the sample was washed with solutions of sodium deoxycholate (SDC), a strong surfactant known to displace noncovalently bound ssDNA on the SWCNT surface.[24] Covalent reaction at the single guanine site of $T_{15}GT_{15}$ is signaled by clear red-shifts in E_{11} emission and absorption, as well as an increase in the Raman D/G intensity ratio that indicates the conversion of some sp^2-hybridized carbon atoms into sp^3 sites. Although SDC molecules in the final wash will adsorb to exposed surfaces of the functionalized SWCNTs and may disturb the adsorption of non-covalently bound ssDNA, we do not expect them to affect the electronic perturbations from guanine covalent bonding. These observations show that ssDNA oligos with 31 nucleotides can be covalently anchored to SWCNT sidewalls by a single guanine. To assess the (*n*,*m*)-specific emission spectral shifts, we analyzed sample fluorescence spectra as superpositions of Voigt functions representing the underlying (*n*,*m*) spectral components, using the fitting approach developed previously (see Figures1b and S2).[25,26]

We performed a parallel study of spectral shifts in guanine-functionalized SWCNTs coated by $T_{30}G$ oligos. Figure 2a shows the emission spectra for treated SWCNTs coated with $T_{30}G$ and $T_{15}GT_{15}$ ssDNA oligos. Although both of these contain the same fraction of guanine bases (1 out of 31), the spectral shifts with $T_{15}GT_{15}$ are substantially larger than with $T_{30}G$. We also find a higher Raman D/G intensity ratio in the treated samples with $T_{15}GT_{15}$ compared to $T_{30}G$, confirming that the larger emission spectral shift reflects a higher density of covalently

functionalized sites in the nanotube (see Figure 2b). Because the two oligos have the same guanine fraction (1/31), these results imply a higher probability for the ssDNA guanine base to react with the nanotube sidewall when it is located in the center of the strand.

To further explore this effect, we prepared additional SWCNT samples dispersed in solutions of GT_{30}, $T_{29}GT$, $T_{28}GT_2$, $T_{24}GT_6$, $T_{21}GT_9$, and $T_{18}GT_{12}$. These ssDNA oligos all contain 30 thymine bases and one guanine base and can be represented as $T_{31-n}GT_{n-1}$, in which the guanine position ranges from the end, for n = 1 or 31, to the center, for n = 16. We observe that the spectral shifts in these treated nanotubes depend monotonically on the guanine position in the ssDNA oligos that coat them (see Figure 3). Greater red shifts occur with n values nearer to 16, indicating enhanced covalent functionalization density when the guanine nucleotide is located closer to the center of the strand. Using the nearly proportional empirical correlation between guanine fraction and E_{11} spectral shift found previously,[15] we deduced the apparent guanine fractions in $T_{31-n}GT_{n-1}$ oligos by analyzing fluorescence spectra measured before and after the singlet oxygen treatment (see Figures S4 and S5). The results are plotted in Figure 3a as apparent guanine fraction *vs*. guanine position. (To minimize possible effects from (n,m)-dependent ssDNA wrapping and reactivity, we show apparent fractions averaged over the (6,5), (7,5), and (7,6) species − see Table S1). The apparent guanine fraction increases monotonically from ca. 1.9 to 6.2% as the guanine position varies from the end to the center of $T_{31-n}GT_{n-1}$ oligos. Because $T_{15}GT_{15}$ shows an apparent guanine fraction almost twice its actual fraction of 3.2%, we infer that the centers of adjacent $T_{15}GT_{15}$ ssDNA strands are positioned much closer together along the SWCNT axis than would occur if their tails remained fully adsorbed onto the nanotube. Note that our reference relation between guanine fraction and spectral shifts was deduced from “calibration” measurements on

oligos such as $(TGT)_{15}$, in which guanine sites are uniformly and densely spaced along the strand. The reference relation should therefore be unaffected by any partial strand desorption.

We performed further experiments to see if lower concentrations of free $T_{15}GT_{15}$ ssDNA affected its apparent wrapping density on SWCNTs. Figure 3b shows the spectral shifts measured after guanine functionalization with several free ssDNA concentrations. We found that diluting the free $T_{15}GT_{15}$ concentration by a factor of 4 gave a decrease in apparent guanine fraction from ca. 6.2% to 2.8% (near the expected statistical value). This suggests that the initial mass concentration of ssDNA, which was approximately 7 times that of the SWCNT prior to dispersion, led to approximately twice the density of adsorbed guanine bases compared to the 4x diluted sample. Such a higher density might result from crowding-induced partial desorption of the oligo tails while the central regions with guanines remained less perturbed. For oligos with guanines located near the ends, surface crowding at high concentrations of free ssDNA might induce the guanines to partially desorb or reorient relative to the SWCNT surface, causing a decrease in their reactivity. A reduced concentration of free ssDNA would then avoid crowding on the nanotube surface and the associated partial ssDNA desorption, allowing the apparent guanine fraction to approach the true value.

We complemented the experimental study with atomistic molecular dynamics (MD) simulations of $T_{30}G$ and $T_{15}GT_{15}$ oligos wrapped around (6,5) SWCNTs. Previous studies have shown that both standard MD simulations and enhanced sampling methods provide valuable information about ssDNA interactions with SWCNTs.[27–30] Here we modeled a 20 nm long segment of a (6,5) nanotube wrapped with three adjacent strands of ssDNA to observe effects on the central strand from interactions with the strands on both sides. Crowding among these strands was simulated by steering the left and right strands toward the central one with an external axial force

constant of 1 kcal mol^{-1} $Å^{-2}$ applied to their outer end regions, highlighted in yellow in Figure 4a.[31] The axial length (projection along the SWCNT axis) between centers of the outermost bases in the three-strand system was thereby compressed from 15.8 nm to 10.5 nm over a period of 100 ns. At various stages of the compression, several thousand MD snapshots were analyzed to find the radial distances between the SWCNT axis and all nucleobases in the central strand. We then averaged these radial distance values for the 4 nucleobases nearest to the strand center and for the 4 nearest to the strand ends and plotted the distances versus the center strand's axial length to construct Figure 4b. For both regions within the central strand, compression tends to increase the average radial distances as inter-strand repulsions disrupt some of the π–π stacking interactions keeping nucleobases adsorbed to the SWCNT surface. This crowding desorption effect is clearly stronger for bases near the strand ends than for those near its middle.

To further examine interactions between adjacent ssDNA strands, we simulated a more rapid axial compression to 10.5 nm of the three-strand $T_{15}GT_{15}$ / (6,5) system followed by 90 ns of static condition MD trajectories, from which 4000 snapshots were analyzed to obtain the radial distances of all nucleobases. The averages and standard deviations of these distances are plotted in Figure 4c as a function of base position from end to center, along with equivalent averages for a single strand of $T_{15}GT_{15}$ without neighbors on a (6,5) segment. We find that crowding from adjacent strand interactions leads to increased desorption tendency, particularly for nucleobases near the ends of the middle strand. This position-dependent desorption trend is generally consistent with the interpretation of our experimental spectroscopic findings described above, assuming that guanine bases that are not in close contact with the SWCNT surface are less likely to undergo the covalent functionalization reaction. It also seems possible that ssDNA desorption at strand ends might enhance the complexation of rose bengal sensitizer molecules with the nanotube.

Our combined experimental and computational results suggest that suspending SWCNTs in common concentrations of dissolved ssDNA can lead to repulsive interactions between neighboring adsorbed ssDNA strands. We find spectral evidence that guanine nucleobases exposed to $^1O_2$ react more readily with the nanotube surface when they are located at the center of the ssDNA strand than at or near the strand end. In addition, the inferred high functionalization density from using strands containing central guanine bases points to a closer packing of the strand centers, as is also consistent with partial desorption of the ends. It is not yet clear whether this effect will occur for all ssDNA coatings, some of which may be stabilized by inter-strand hydrogen bonding. We expect that further studies of base sequence-dependent guanine functionalization effects will lead to improved understanding of ssDNA-SWCNT hybrids and advance their use in research and applications.

ASSOCIATED CONTENT

Supporting Information. Methods for sample preparation and functionalization; details of computational methods; additional plots and tables of spectral data. This material is available free of charge via the Internet at http://pubs.acs.org.

AUTHOR INFORMATION

Corresponding Author

* E-mail: weisman@rice.edu.

ORCID

Yu Zheng: 0000-0003-2703-9143

Ali A. Alizadehmojarad: 0000-0001-6806-5415

Sergei M. Bachilo: 0000-0001-5236-1383

R. Bruce Weisman: 0000-0001-8546-9980

Present Address

[§] Center for Integrated Nanotechnologies, Materials Physics and Applications Division, Los Alamos National Laboratory, Los Alamos, New Mexico 87545, United States

Notes

The authors declare the following competing financial interest: R. B. W. has a financial interest in Applied NanoFluorescence, LLC, which manufactures some of the instruments used in this project.

ACKNOWLEDGMENTS

This research was supported by grants from the National Science Foundation (CHE-1803066) and the Welch Foundation (C-0807).

REFERENCES

(1) Reich, S.; Thomsen, C.; Maultzsch, J. *Carbon Nanotubes: Basic Concepts and Physical Properties*; John Wiley & Sons: Hoboken, 2008.

(2) Zheng, M.; Jagota, A.; Semke, E. D.; Diner, B. A.; McClean, R. S.; Lustig, S. R.; Richardson, R. E.; Tassi, N. G. DNA-Assisted Dispersion and Separation of Carbon Nanotubes. *Nat. Mater.* **2003**, *2*, 338–342.

(3) Zheng, M.; Jagota, A.; Strano, M. S.; Santos, A. P.; Barone, P.; Chou, S. G.; Diner, B. A.; Dresselhaus, M. S.; Mclean, R. S.; Onoa, G. B.; Samsonidze, G. G.; Semke, E. D.; Usrey, M.; Walls, D. J. Structure-Based Carbon Nanotube Sorting by Sequence-Dependent DNA Assembly. *Science* **2003**, *302* (5650), 1545–1548.

(4) Tu, X.; Manohar, A.; Jagota, A.; Zheng, M. DNA Sequence Motifs for Structure-Specific Recognition and Separation of Carbon Nanotubes. *Nature* **2009**, *460*, 250–253.

(5) Ao, G.; Khripin, C. Y.; Zheng, M. DNA-Controlled Partition of Carbon Nanotubes in Polymer Aqueous Two-Phase Systems. *J. Am. Chem. Soc.* **2014**, *136*, 10383–10392.

(6) Barone, P. W.; Baik, S.; Heller, D. A.; Strano, M. S. Near-Infrared Optical Sensors Based on Single-Walled Carbon Nanotubes. *Nat. Mater.* **2005**, *4*, 86–92.

(7) Jena, P. V.; Roxbury, D.; Galassi, T. V.; Akkari, L.; Horoszko, C. P.; Iaea, D. B.; Budhathoki-Uprety, J.; Pipalia, N.; Haka, A. S.; Harvey, J. D.; Mittal, J.; Maxfield, F. R.; Joyce, J. A.; Heller, D. A. A Carbon Nanotube Optical Reporter Maps Endolysosomal Lipid Flux. *ACS Nano* **2017**, *11*, 10689–10703.

(8) Kruss, S.; Hilmer, A. J.; Zhang, J.; Reuel, N. F.; Mu, B.; Strano, M. S. Carbon Nanotubes as Optical Biomedical Sensors. *Adv. Drug Deliv. Rev.* **2013**, *65*, 1933–1950.

(9) Williams, R. M.; Lee, C.; Galassi, T. V.; Harvey, J. D.; Leicher, R.; Sirenko, M.; Dorso, M. A.; Shah, J.; Olvera, N.; Dao, F.; Levine, D. A.; Heller, D. A. Noninvasive Ovarian Cancer Biomarker Detection via an Optical Nanosensor Implant. *Sci. Adv.* **2018**, *4*.

(10) Williams, R. M.; Lee, C.; Heller, D. A. A Fluorescent Carbon Nanotube Sensor Detects the Metastatic Prostate Cancer Biomarker UPA. *ACS Sens.* **2018**, *3*, 1838–1845.

(11) Boghossian, A. A.; Zhang, J.; Barone, P. W.; Reuel, N. F.; Kim, J.-H.; Heller, D. A.; Ahn, J.-H.; Hilmer, A. J.; Rwei, A.; Arkalgud, J. R.; Zhang, C. T.; Strano, M. S. Near-Infrared Fluorescent Sensors Based on Single-Walled Carbon Nanotubes for Life Sciences Applications. *ChemSusChem* **2011**, *4*, 848–863.

(12) Langenbacher, R.; Budhathoki-Uprety, J.; Jena, P. V.; Roxbury, D.; Streit, J.; Zheng, M.; Heller, D. A. Single-Chirality Near-Infrared Carbon Nanotube Sub-Cellular Imaging and FRET Probes. *Nano Lett.* **2021**, *21*, 6441–6448.

(13) Sun, W.; Shen, J.; Zhao, Z.; Arellano, N.; Rettner, C.; Tang, J.; Cao, T.; Zhou, Z.; Ta, T.; Streit, J. K.; Fagan, J. A.; Schaus, T.; Zheng, M.; Han, S.-J.; Shih, W. M.; Maune, H. T.;

Yin, P. Precise Pitch-Scaling of Carbon Nanotube Arrays within Three-Dimensional DNA Nanotrenches. *Science* **2020**, *368*, 874–877.

(14) Zhao, M.; Chen, Y.; Wang, K.; Zhang, Z.; Streit, J. K.; Fagan, J. A.; Tang, J.; Zheng, M.; Yang, C.; Zhu, Z.; Sun, W. DNA-Directed Nanofabrication of High-Performance Carbon Nanotube Field-Effect Transistors. *Science* **2020**, *368*, 878–881.

(15) Zheng, Y.; Bachilo, S. M.; Weisman, R. B. Controlled Patterning of Carbon Nanotube Energy Levels by Covalent DNA Functionalization. *ACS Nano* **2019**, *13*, 8222–8228.

(16) Zheng, Y.; Kim, Y.; Jones, A. C.; Olinger, G.; Bittner, E. R.; Bachilo, S. M.; Doorn, S. K.; Weisman, R. B.; Piryatinski, A.; Htoon, H. Quantum Light Emission from Coupled Defect States in DNA-Functionalized Carbon Nanotubes. *ACS Nano* **2021**, *15*, 10406–10414.

(17) Ghosh, S.; Bachilo, S. M.; Simonette, R. A.; Beckingham, K. M.; Weisman, R. B. Oxygen Doping Modifies Near-Infrared Band Gaps in Fluorescent Single-Walled Carbon Nanotubes. *Science* **2010**, *330*, 1656–1659.

(18) Piao, Y.; Meany, B.; Powell, L. R.; Valley, N.; Kwon, H.; Schatz, G. C.; Wang, Y. Brightening of Carbon Nanotube Photoluminescence through the Incorporation of sp^3 Defects. *Nat. Chem.* **2013**, *5*, 840–845.

(19) Zheng, Y.; Bachilo, S. M.; Weisman, R. B. Photoexcited Aromatic Reactants Give Multicolor Carbon Nanotube Fluorescence from Quantum Defects. *ACS Nano* **2020**, *14*, 715–723.

(20) Kwon, H.; Furmanchuk, A.; Kim, M.; Meany, B.; Guo, Y.; Schatz, G. C.; Wang, Y. Molecularly Tunable Fluorescent Quantum Defects. *J. Am. Chem. Soc.* **2016**, *138*, 6878–6885.

(21) Shiraki, T.; Shiraishi, T.; Juhász, G.; Nakashima, N. Emergence of New Red-Shifted Carbon Nanotube Photoluminescence Based on Proximal Doped-Site Design. *Sci. Rep.* **2016**, *6*, 28393.

(22) Maeda, Y.; Takehana, Y.; Yamada, M.; Suzuki, M.; Murakami, T. Control of the Photoluminescence Properties of Single-Walled Carbon Nanotubes by Alkylation and Subsequent Thermal Treatment. *Chem. Commun.* **2015**, *51*, 13462–13465.

(23) Brozena, A. H.; Kim, M.; Powell, L. R.; Wang, Y. H. Controlling the Optical Properties of Carbon Nanotubes with Organic Colour-Centre Quantum Defects. *Nat. Rev. Chem.* **2019**, *3*, 375–392.

(24) Zheng, Y.; Bachilo, S. M.; Weisman, R. B. Enantiomers of Single-Wall Carbon Nanotubes Show Distinct Coating Displacement Kinetics. *J. Phys. Chem. Lett.* **2018**, *9*, 3793–3797.

(25) Rocha, J. D.; Bachilo, S. M.; Ghosh, S.; Arepalli, S.; Weisman, R. B. Efficient Spectrofluorimetric Analysis of Single-Walled Carbon Nanotube Samples. *Anal. Chem.* **2011**, *83*, 7431–7437.

(26) Weisman, R. B. Fluorimetric Characterization of Single-Walled Carbon Nanotubes. *Anal. Bioanal. Chem.* **2010**, *396*, 1015–1023.

(27) Johnson, R. R.; Johnson, A. T. C.; Klein, M. L. Probing the Structure of DNA−Carbon Nanotube Hybrids with Molecular Dynamics. *Nano Lett.* **2008**, *8*, 69–75.

(28) Beyene, A. G.; Alizadehmojarad, A. A.; Dorlhiac, G.; Goh, N.; Streets, A. M.; Král, P.; Vuković, L.; Landry, M. P. Ultralarge Modulation of Fluorescence by Neuromodulators in Carbon Nanotubes Functionalized with Self-Assembled Oligonucleotide Rings. *Nano Lett.* **2018**, *18*, 6995–7003.

(29) Alizadehmojarad, A. A.; Zhou, X.; Beyene, A. G.; Chacon, K. E.; Sung, Y.; Pinals, R. L.; Landry, M. P.; Vuković, L. Binding Affinity and Conformational Preferences Influence Kinetic Stability of Short Oligonucleotides on Carbon Nanotubes. *Adv. Mater. Interfaces* **2020**, *7*, 2000353.

(30) Roxbury, D.; Mittal, J.; Jagota, A. Molecular-Basis of Single-Walled Carbon Nanotube Recognition by Single-Stranded DNA. *Nano Lett.* **2012**, *12*, 1464–1469.

(31) Isralewitz, B.; Gao, M.; Schulten, K. Steered Molecular Dynamics and Mechanical Functions of Proteins. *Curr. Opin. Struct. Biol.* **2001**, *11*, 224–230.

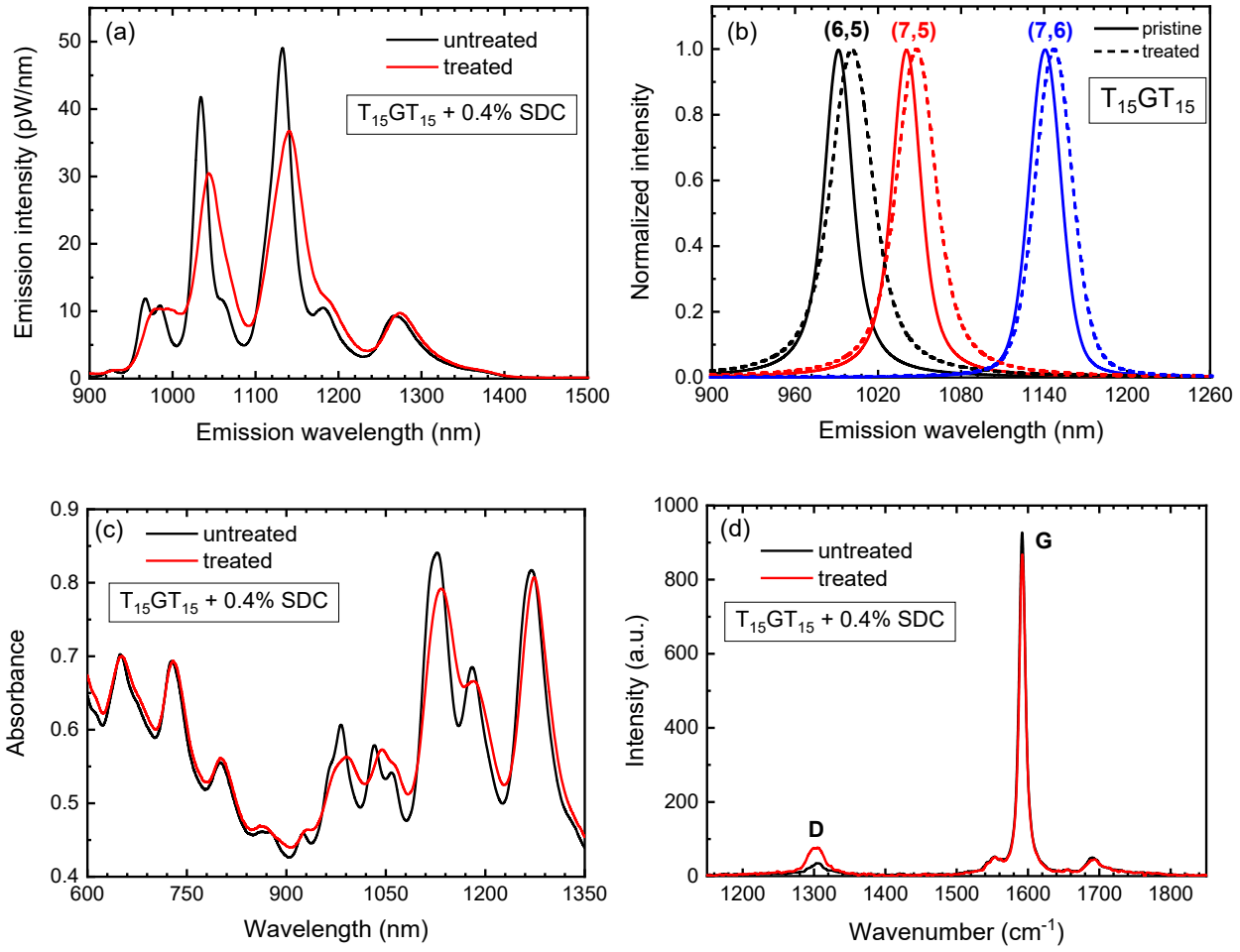

Figure 1. (a) Fluorescence spectra of SWCNTs dispersed in $T_{15}GT_{15}$ ssDNA measured without (black curve) and with (red curve) functionalization treatment. Both samples were coating displaced using 0.4 % SDC before measurement. (b) Simulated emission components from (6,5), (7,5), and (7,6) species before (solid curves) and after (dashed curves) treatment. (c) Absorption and (d) Raman spectra measured without (black curve) and with (red curve) functionalization treatment. Both samples were coating displaced using 0.4 % SDC before measurement.

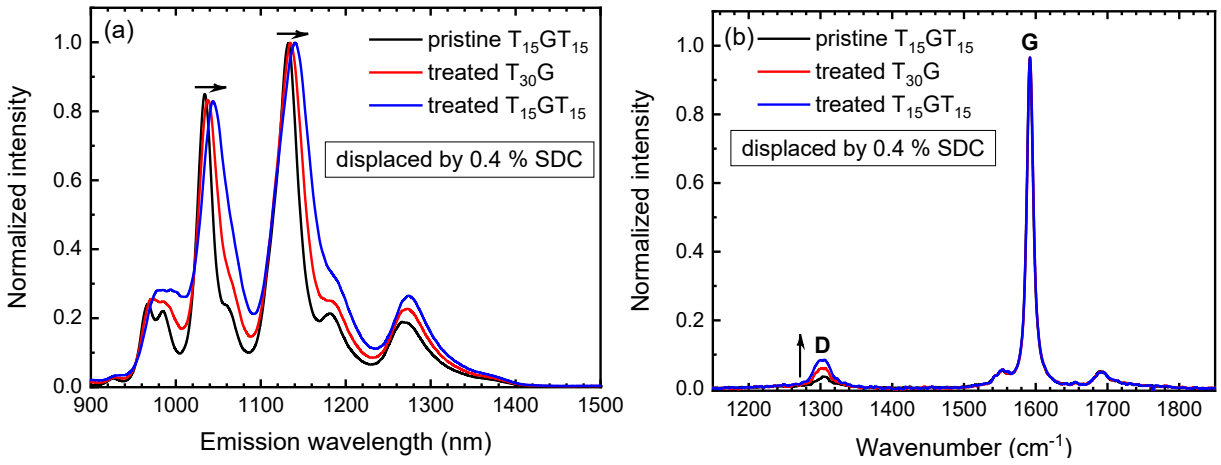

Figure 2. (a) Fluorescence spectra for samples of SWCNTs dispersed with $T_{15}GT_{15}$ and $T_{30}G$ ssDNA oligos. The pristine and treated samples were coating displaced using 0.4% SDC. The black curve shows the spectrum for the pristine sample and the red and blue curves show emission from the treated $T_{30}G$ and $T_{15}GT_{15}$ samples, respectively. (b) Raman spectra for SWCNT samples in (a), normalized to peak G-band intensities.

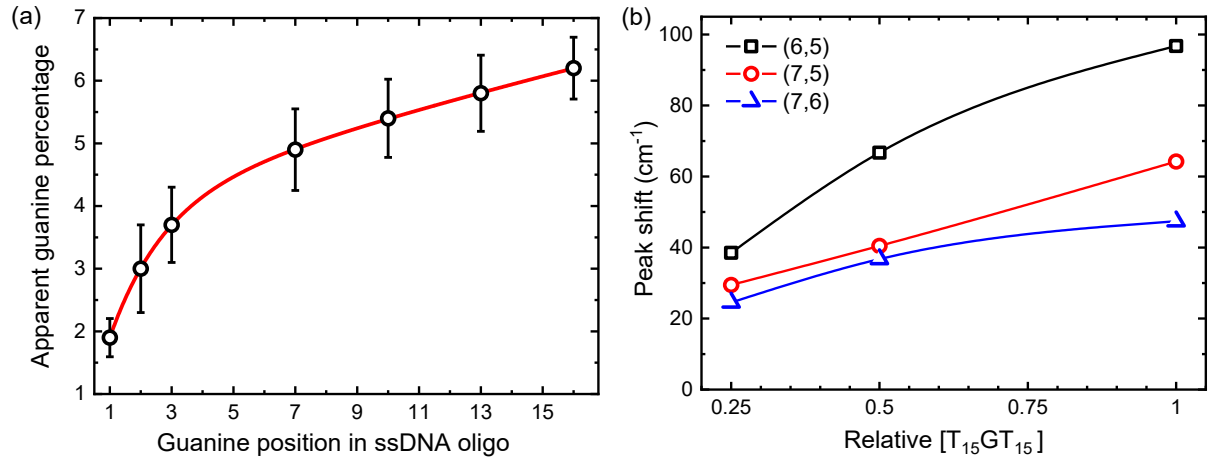

Figure 3. (a) Apparent guanine fraction deduced from spectral shifts in treated SWCNT samples suspended in $T_{31-n}GT_{n-1}$ ssDNA oligos. The x-axis coordinate is the index n describing position of guanine within the oligo (n = 1 is the end position; n = 16 is the center). (b) Plot of E_{11} emission peak shifts for three (n,m) species as a function of relative concentration of the $T_{15}GT_{15}$ oligo in the sample solution. All solutions contained excess dissolved ssDNA in addition to that adsorbed onto SWCNTs.

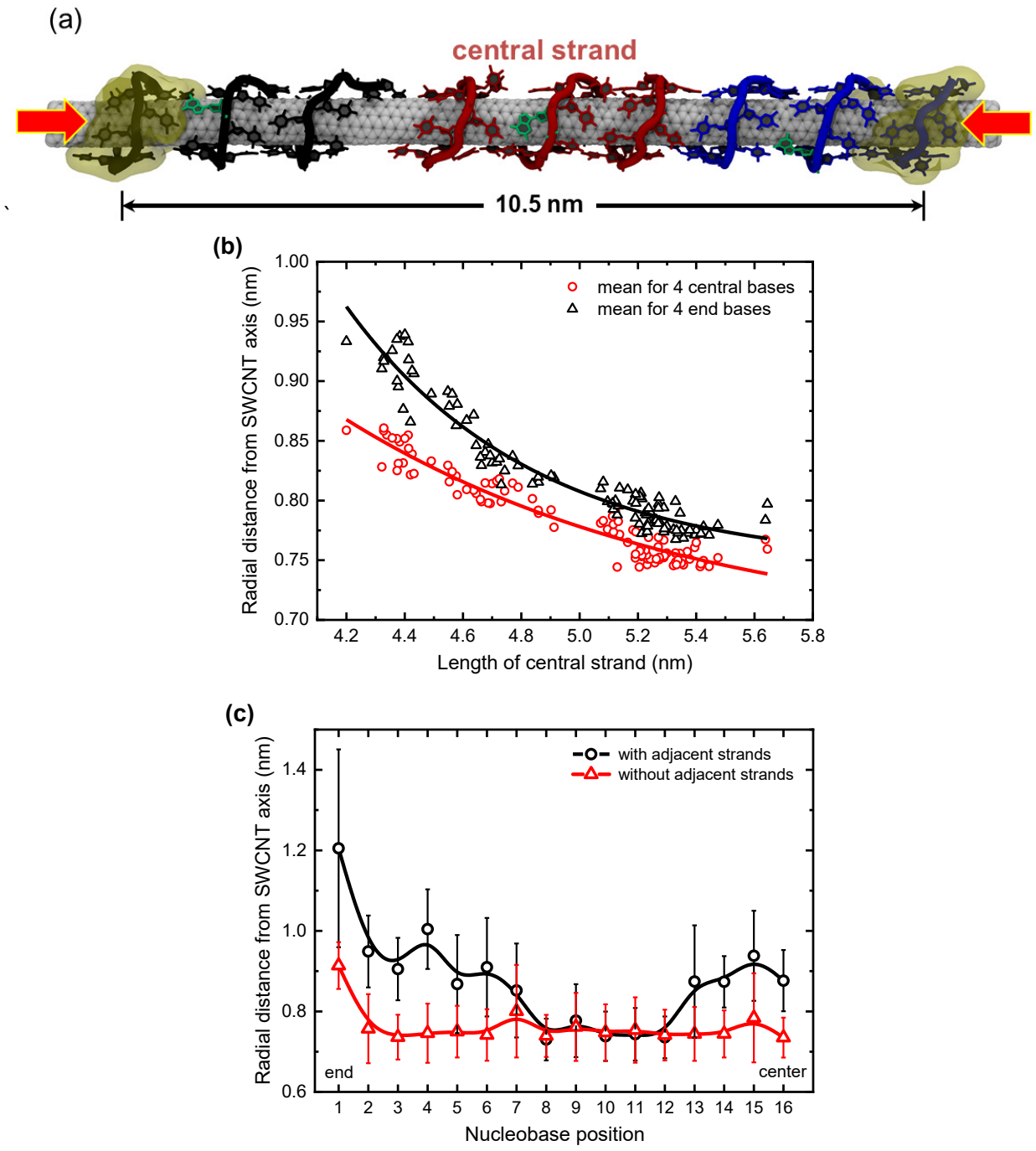

Figure 4. Steered MD simulations of $T_{15}GT_{15}$ ssDNA strands on a (6,5) SWCNT segment. (a) Snapshot structure for three adjacent strands after slow axial compression to reach 10.5 nm between centers of the outermost regions of the outer strands, which are shaded in yellow. Compressive force was applied to the centers of those end regions. The central ssDNA strand is colored red and guanines are colored green. (b) Mean radial distances for the 4 central (red circles) and 4 end bases (black triangles) of the central strand as a function of central strand axial length during compression. Solid lines are curves to guide the eye. (c) Radial distances of bases in the central strand as a function of position within the oligo, shown for the compressed system with adjacent strands (black circles), and for the uncompressed system without adjacent strands (red triangles).